Reconciling plate motion and faulting at a rift-rift-rift triple junction

Daniele Maestrelli[1*], Federico Sani[1,2], Derek Keir[1,3], Carolina Pagli[4], Alessandro La Rosa[4], Ameha Atnafu Muluneh[5,6], Sascha Brune[6,7], Giacomo Corti[2]

[1] Department of Earth Sciences, University of Firenze, Via G. La Pira, 4, 50121, Firenze, Italy,

[2] CNR-IGG, National Research Council of Italy, Institute of Geosciences and Earth Resources, Via G. La Pira 4, 50121,Firenze, Italy

[3] School of Ocean and Earth Science, University of Southampton, University Road, SO17 1BJ, Southampton, UK,

[4] Department of Earth Sciences, University of Pisa, Via Santa Maria, 53, 56126, Pisa, Italy

[5] School of Earth Sciences, Addis Ababa University, P.O. Box 1176, Addis Ababa, Ethiopia

[6] Helmholtz-Centre Potsdam, GFZ German Research Centre for Geosciences, Wissenschaftpark "Albert Einstein", Telegrafenberg, 14473, Potsdam, Germany

[7] Institute of Geosciences, University of Potsdam, Karl-Liebknecht-Str. 24-25, 14476 Potsdam, Germany

ABSTRACT

Rift-Rift-Rift triple junctions are regions where three plates interact generating complex networks of variably oriented faults. While the geometry of the fault networks is easily constrained from their surface expression, what remains unclear is how the kinematics of faults and their interactions vary spatially, and how these relate to the unusual crustal motions that results from three plates diverging from each other. The Afar depression lies at the triple junction between the African, Arabian and Somalian plates where the unique combination of observational data from structural mapping, seismicity, and GNSS allows to understand the link between fault kinematics and plate motions. Here we complement these observations with an analog model to gain insights into how the patterns and directions of faults relate to overall plate motions. A key finding in both model and nature is that some adjacent normal faults form at high angles and generate T-shaped structures. These purely normal faults are synchronously active, which means that the extension direction varies ~90° locally. These kinematic contrasts in model and nature occur despite the relatively smooth pattern of overall surface motions. The results indicate that normal faults interacting at high angles to form the T-shaped structures can evolve synchronously within a stress field that varies gently in magnitude but dramatically in orientation over a few kilometers.

INTRODUCTION

Divergent triple junctions involve the movement of three tectonic plates away from each other (McKenzie & Morgan, 1969), resulting in a fault network that is very complex and may display variation in space and time. However, extensional triple junctions are difficult to observe and analyze in detail, since they most commonly develop in oceanic lithosphere (Ridge-Ridge-Ridge triple junctions) below sea level (McKenzie & Morgan, 1969). The Afar triple junction (Fig. 1A) is the only extensional triple junction directly observable subaerially (Varet, 2018). Extension has not reached the oceanic stage yet in Afar, where the continental lithosphere is still breaking apart giving rise to a Rift-Rift-Rift triple junction. The structural pattern in the region is characterized by atypical fault architecture (curvilinear, overlapping and cross-cutting faults), kinematics (oblique and/or strike-slip faulting) and interactions (T-shaped plan-view fault geometries). Similarly, T-axes of earthquake focal mechanisms and the orientation of dikes in and around the triple junction commonly vary by ~90º over distances of tens of km, indicating that they likely respond to local complexities in stress direction (e.g., Keir et al. 2011; Doubre et al., 2017). Overall, the processes that control the geometry, interaction and kinematics of faults, and their relationship to the spatially variable and complex pattern of extension resultant from 3 diverging plates remain poorly understood (Rime et al., 2023). Here we compare an analog model with observations from the Afar depression (structural trends, GNSS data and T-axes from earthquakes) to gain insights into the distribution and kinematics of the complex deformation processes.

THE AFAR TRIPLE JUNCTION

The Afar triple junction results from the movement among the African, Somalian, and Arabian plates (e.g., Burke & Dewey, 1973; Hayward & Ebinger, 1996; Manighetti et al., 1997; Tesfaye et al., 2003; Wolfenden et al., 2004). The African and Somalian plates move apart at ~5 mm/yr in an ESE-WNW direction (Saria et al., 2014; Knappe et al., 2020; Stamps et al., 2021), giving rise to a system of NE-SW-trending faults representing the northward termination of the Main Ethiopian Rift (Fig. 1A). Conversely, the ~20 mm/yr northeastward motion of the Arabian plate relative to Africa and Somalia (McClusky et al., 2010), results in the development of NW-SE-trending faults in the Afar rift segments that are related to Red Sea and Gulf of Aden opening (Fig. 1A). These two main fault systems interact in central Afar, developing typical T-shaped structures, with sharp 90° fault interactions. Previously, the region where the T-shaped structures are most pronounced has been interpreted as where the mutually perpendicular extension generated by plate motion is believed to be partitioned, and therefore where the triple junction is positioned (Maestrelli et al., 2022; Fig. 1A,B). However, the combination of observational and modelling studies suggests the diverging

plates may interact across a wider (several hundred km-wide) zone. For example, the major curvilinear or Y-shaped grabens coupled with minor perpendicular faults in eastern Afar (e.g., Immino graben; IM in Fig. 1A), and rift perpendicular dike intrusion in southern Afar, are best explained by a broad zone of triple junction tectonics (Keir et al., 2011; Collanega et al., 2020; Fig. S1).

DATA AND METHODS

Analog model

We performed analog models reproducing the dynamics of a RRR triple junction by simulating the motion of three tectonic plates (Africa, Arabia, Somalia) diverging from each other. To get detailed insights into the deformation of the Afar triple junction, we used the best-fit model from Maestrelli et al., 2022 (Model A-OR-6, see Supplementary material for setup details, Fig. S2) involving simulation of two-phase motion among the three plates. The first phase implies NE motion of Arabia with respect to stable Africa-Somalia; the second phase involves contemporaneous ESE-WNW divergence of Africa and Somalia and accelerated NE motion of Arabia (e.g., Tesfaye et al., 2003; see Supplementary material, Fig. S2; the influence of different extension conditions was tested in Maestrelli et al., 2022). During this last phase, Arabia is moving four times faster than Africa and Somalia (i.e., R=4 where R is the velocity ratio $|V_{Arabia}|/|V_{Africa=Somalia}|$), as currently occurring in the natural system (McClusky et al., 2010). This model well accounts for the overall structural features and evolution of deformation in Afar, with a progressive northward migration of the structural triple junction and depocenter with time (see Maestrelli et al., 2022). We performed a detailed analysis of fault patterns, kinematics of deformation and dynamics of fault interaction. Model deformation was monitored through top-view photos and digital elevation models through photogrammetry. We analyzed model displacement fields through Particle Image Velocimetry (PIV) with the PIVlab software (Thielicke and Stamhuis, 2014; see Supplementary material for details). Additionally, by monitoring the motion of markers in the footwall and the hangingwall on individual faults, we provide an indication of the direction of extensional slip across the specific fault (Philippon et al., 2015). We call these the model T-axes since the measurements are analogous to the T-axes derived from earthquake focal mechanisms.

Fault analysis

Both in nature and the model, statistical analysis was performed on fault segments by using the FracPaQ tool for MATLAB™ (Healy et al., 2017). Trends of fault segments in the model were plotted using rose diagrams (10° bin) and compared with the trends of natural faults mapped on a 30m

resolution SRTM Digital Elevation Model (Farr et al., 2007; free to download at https://earthexplorer.usgs.gov/) at the triple junction area (Figs. 1B,C and 2B,C). Regional fault mapping was performed at 1:250.000 scale.

GNSS based rift motions

We derived the 2D velocity field of the Afar triple junction by interpolating two-dimensional GNSS velocities in an Africa-fixed reference frame (Doubre et al., 2017) onto a uniform grid with 19 km spacing that is equivalent to the scaled grid size of the analog model (Fig. 4). To obtain the long-term velocity field, we removed GNSS based velocities near the Dabbahu segment where a rifting episode occurred in 2005-2010 (Wright et al., 2012). Since GNSS sites on the Somalia plate are scarce, we fixed site velocities for three additional points on the Somalian Plate assuming the values predicted by Stamps et al. (2008).

Earthquake T-axes and dike opening directions

We derive T-axes from the global Centroid Moment Tensor (gCMT) catalog for the region (time period 1976-2022, Ekström et al., 2012; last accessed October 2023). In addition, we compiled a database of dike locations and their strike modelled from InSAR observations (Goitom et al., 2015; Moore et al., 2019; Keir et al., 2009; Nobile et al, 2012; Pagli et al., 2012; Tarantola et al., 1980; Wright et al., 2006), and derived the opening direction (orthogonal to the strike) of each dike.

RESULTS

Fault pattern

A detailed analysis of the analog model indicates a very good correspondence with Afar in terms of fault pattern (cf. Figs. 1, 2; see also Fig. S3). The model reproduces the two dominant fault sets characterizing Afar: the NW-SE-trending faults, related to NE motion of Arabia, and the roughly NE-SW-trending extensional structures related to the relative divergence of the African and Somalian plates. The statistical analysis of fault orientations in the model highlights the two dominant fault sets, as illustrated in Figure 2C. The NE-SW-directed faults in the model define a series of sub-parallel grabens closely resembling the major sub-parallel basins of Afar (Figs. 1, 2). A closer view of the fault pattern at the triple junction reveals the two sets of faults interacting at a high angle (Fig. 2B), giving rise to a T-shaped pattern of extensional structures which also characterize central Afar (Fig. 1). Detailed analysis of the evolution of faulting at the analog model triple junction (Fig. 3) reveals that faults interact at high angles and form the T-shaped structures contemporaneously. Analysis of

the analog model T-axes clearly indicates that two roughly orthogonal directions of extension (NE-SW-trending and roughly E-W-directed) are responsible for the development of these faults (Fig. 3).

Plate motions and kinematics of faulting

Figure 4 compares the modelled surface velocities to those measured by GNSS, showing the overall kinematics of the plates. In general, there is a good match between modelled and GNSS-derived surface velocities (Fig. 4A), with the discrepancies generally lower than 15° and with better correlation where the GNSS data is denser. Similarly, the indicators of fault extension from the T-axes of earthquakes and those calculated from the analog model match very well (Fig. 4B). These primarily trend NE in northern and central Afar, but show both NE and ESE directions in southern Afar (Fig. 4B). In contrast to the plate motions however, these indicators of extension vary over very short length scales – a few tens of kilometers. The earthquake T-axes are also similar to the dike opening directions, suggesting that extension across the faults is similar to the direction of minimum horizontal stress (σ_3). The similarity between earthquake T-axes and dike opening direction also shows faults and dikes are responding in a similar way to both regional and local stresses.

DYNAMICS OF FAULT INTERACTION AT RIFT-RIFT-RIFT TRIPLE JUNCTIONS (AND IMPLICATIONS FOR AFAR)

The very good match between the analog model and the Afar depression suggests that the overall deformation pattern and its evolution result from different stress fields related to the differential divergent motion acting contemporaneously at the triple junction (e.g., Rime et al., 2023). A key observation from model and nature is that the T-axes can vary by ~90° close to orthogonal fault sets. Such complexity in fault geometry and local orientation of extension is observed within fairly smooth overall surface motions, as indicated from the observed and modelled surface velocity vectors, (Figs. 3, S4) resulting from a dominant NE (Arabia) movement and subordinate NW-SE (Africa-Somalia) divergence. These constraints on both faulting and overall rift motions indicate that faults interacting at high angles to form the T-shaped structures do not result from an alternating stress direction shift over time, but they form and act contemporaneously. These sub-orthogonal fault systems result from the partition of the triple junction's stress field into two roughly orthogonal directions of extension (a NE-SW-trending extension direction related to motion of the Arabian plate and a roughly E-W-directed extension related to Africa-Somalia motion) acting contemporaneously and independently at the triple junction, as suggested for others extensional settings (e.g., the Barents Sea, Collanega et al., 2020). This process explains the anomalous WNW-ESE dike intrusion occurred during May 2000 in the Main Ethiopian Rift of southern Afar (Ayelu-Amoissa Dike, AAD in Fig. 4B). The dike event

documents NE-SW directed extension, roughly perpendicular to the dominant near ESE-WNW extension related to Africa-Somalia motion (Keir et al., 2011). Coexistence of the Africa-Arabia-related stress field in the area, as suggested by model analysis and the resulting partition of deformation, may explain this anomalously oriented dike event and the associated seismicity (Fig. S1). In addition to the dominance of T-shaped structures, other complex graben geometries (e.g., curvilinear and Y-shaped grabens) are also observed in Afar (Collanega et al., 2020) and can be explained by our model.

Traditionally, complex patterns of fault trends and slip directions (e.g., angular or T-shaped patterns) have been interpreted as resulting from a multiphase evolution with changes in time of the regional extension direction (see discussion in Zwaan et al. 2021). This allows multiple fault sets to be activated at different times and for temporal variability in fault slip to occur. Our observations do not support this scenario for the current tectonics of Afar, but instead show that highly variable fault orientations but with normal slip kinematics can be synchronously active. The magnitude of horizontal principal stresses (σ_2 and σ_3) are prone to being similar at a multi-directionally divergent zone like Afar. This facilitates that σ_2 and σ_3 switch locally, generating a 90° shift in the fault orientation and slip directions. This finding indicates caution should be used when interpreting the behavior of interacting fault systems from time-averaged structural data in these complex structural settings.

ACKNOWLEDGMENTS

We thank three Reviewers and the Editor Rob Strachan for the constructive comments. This work was supported by Ministero dell'Università e della Ricerca (MiUR) through PRIN Grant 2017P9AT72. We acknowledge the support of the JRU EPOS Italia.

REFERENCES CITED

Burke, K., & Dewey, J. F. 1973. Plume-generated triple junctions: Key indicators in applying plate tectonics to old rocks. The Journal of Geology, 81(4), 406–433. https://doi.org/10.1086/627882

Collanega, L., Corti, G., Breda, A., Massironi, M., & Keir, D. 2020. 3D extension at plate boundaries accommodated by interacting fault systems. Scientific Reports, 10(1), 8669.

Doubre, C., Deprez, A., Masson, F., Socquet, A., Lewi, E., Grandin, R., ... & Wright, T. 2017. Current deformation in Central Afar and triple junction kinematics deduced from GPS and InSAR measurements. Geophysical Journal International, 208(2), 936-953.

Ekström, G., M. Nettles, and A. M. Dziewonski, 2012. The global CMT project 2004-2010: Centroid-moment tensors for 13,017 earthquakes, Physics of the Earth and Planetary Interiors, 200-201, 1-9. doi:10.1016/j.pepi.2012.04.002

Farr, T. G., Rosen, P. A., Caro, E., Crippen, R., Duren, R., Hensley, S., ... & Alsdorf, D. (2007). The shuttle radar topography mission. Reviews of geophysics, 45(2). https://doi.org/10.1029/2005RG000183

Goitom, B., Oppenheimer, C., Hammond, J.O.S. et al. 2015. First recorded eruption of Nabro volcano, Eritrea, 2011. Bulletin of Volcanology, 77, 85. https://doi.org/10.1007/s00445-015-0966-3

Hayward, N. J., & Ebinger, C. J. 1996. Variations in the along-axis segmentation of the Afar Rift system. Tectonics, 15(2), 244–257. https://doi.org/10.1029/95TC02292

Healy, D., Rizzo, R. E., Cornwell, D. G., Farrell, N. J., Watkins, H., Timms, N. E., et al. 2017. FracPaQ: A MATLAB™ toolbox for the quantification of fracture patterns. Journal of Structural Geology, 95, 1–16. https://doi.org/10.1016/j.jsg.2016.12.003

Keir, D., Hamling, I. J., Ayele, A., Calais, E., Ebinger, C., Wright, T. J., ... & Bennati, L. 2009. Evidence for focused magmatic accretion at segment centers from lateral dike injections

captured beneath the Red Sea rift in Afar. Geology, 37(1), 59-62. https://doi.org/10.1130/G25147A.1

Keir, D., Pagli, C., Bastow, I. D., & Ayele, A. 2011. The magma-assisted removal of Arabia in Afar: Evidence from dike injection in the Ethiopian rift captured using InSAR and seismicity. Tectonics, 30(2). https://doi.org/10.1029/2010TC002785

Keir, D., Bastow, I. D., Pagli, C., & Chambers, E. L. 2013. The development of extension and magmatism in the Red Sea rift of Afar. Tectonophysics, 607, 98–114. https://doi.org/10.1016/j.tecto.2012.10.015

Knappe, E., Bendick, R., Ebinger, C., Birhanu, Y., Lewi, E., Floyd, M., ... & Perry, M. 2020. Accommodation of East African rifting across the Turkana depression. Journal of Geophysical Research: Solid Earth, 125(2), e2019JB018469. https://doi.org/10.1029/2019JB018469

Maestrelli, D., Bonini, M., Corti, G., Del Ventisette, C., Moratti, G., & Montanari, D. 2021a. A database of laboratory analog models of caldera collapse testing the role of inherited structures. Frontiers in Earth Science, 9, 27. https://doi.org/10.3389/feart.2021.618258

Maestrelli, D., Bonini, M., Corti, G., Del Ventisette, C., Moratti, G., & Montanari, D. 2021b. Exploring fault propagation and the role of inherited structures during caldera collapse through laboratory experiments. Journal of Volcanology and Geothermal Research, 414, 107232. https://doi.org/10.1016/j.jvolgeores.2021.107232

Maestrelli, D., Brune, S., Corti, G., Keir, D., Muluneh, A. A., & Sani, F. 2022. Analog and Numerical Modeling of Rift-Rift-Rift Triple Junctions. Tectonics, 41(10), e2022TC007491. https://doi.org/10.1029/2022TC007491

Manighetti, I., Tapponnier, P., Courtillot, V., Gruszow, S., & Gillot, P. Y. 1997. Propagation of rifting along the Arabia-Somalia plate boundary: The gulfs of Aden and Tadjoura. Journal of Geophysical Research, 102(B2), 2681–2710. https://doi.org/10.1029/96JB01185

255 Manighetti, I., Tapponier, P., Courtillot, V., Gallet, Y., Jacques, E., & Gillot, P. Y. 2001. Strain
256 transfer between disconnected, propagating rifts in Afar. Journal of Geophysical Research,
257 106(B7), 13613–13665. https://doi.org/10.1029/2000JB900454
258 McClusky, S., Reilinger, R., Ogubazghi, G., Amleson, A., Healeb, B., Vernant, P., et al. 2010.
259 Kinematics of the southern Red Sea–Afar Triple Junction and implications for plate dynamics.
260 Geophysical Research Letters, 37(5). https://doi.org/10.1029/2009GL041127
261 McKenzie, D. P., & Morgan, W. J. 1969. Evolution of triple junctions. Nature, 224(5215), 125–133.
262 https://doi.org/10.1038/224125a0
263 Moore, C., Wright, T., Hooper, A., & Biggs, J. 2019. The 2017 Eruption of Erta'Ale Volcano,
264 Ethiopia: Insights into the shallow axial plumbing system of an incipient Mid-Ocean Ridge.
265 Geochemistry, Geophysics, Geosystems, 20(12), 5727-5743.
266 https://doi.org/10.1029/2019GC008692
267 Nobile, A., Pagli, C., Keir, D., Wright, T. J., Ayele, A., Ruch, J., & Acocella, V. 2012. Dike-fault
268 interaction during the 2004 Dallol intrusion at the northern edge of the Erta Ale Ridge (Afar,
269 Ethiopia). Geophysical Research Letters, 39(19). https://doi.org/10.1029/2012GL053152
270 Pagli, C., Wright, T. J., Ebinger, C. J., Yun, S. H., Cann, J. R., Barnie, T., & Ayele, A. 2012. Shallow
271 axial magma chamber at the slow-spreading Erta Ale Ridge. Nature Geoscience, 5(4), 284-
272 288. https://doi.org/10.1038/ngeo1414
273 Philippon, M., Willingshofer, E., Sokoutis, D., Corti, G., Sani, F., Bonini, M., & Cloetingh, S. 2015.
274 Slip re-orientation in oblique rifts. Geology, 43(2), 147-150.
275 https://doi.org/10.1130/G36208.1
276 Rime, V., Foubert, A., Ruch, J., & Kidane, T. 2023. Tectonostratigraphic evolution and significance
277 of the Afar Depression. Earth-Science Reviews, 104519.
278 https://doi.org/10.1016/j.earscirev.2023.104519

279 Saria, E., Calais, E., Stamps, D. S., Delvaux, D., & Hartnady, C. J. H. 2014. Present-day kinematics
280 of the East African Rift. Journal of Geophysical Research: Solid Earth, 119(4), 3584–3600.
281 https://doi.org/10.1002/2013JB010901
282 Stamps, D. S., Kreemer, C., Fernandes, R., Rajaonarison, T. A., & Rambolamanana, G. 2021.
283 Redefining east African rift system kinematics. Geology, 49(2), 150-155.
284 https://doi.org/10.1130/G47985.1
285 Tarantola, A., Ruegg, J-C., and Lepine, J-C. 1980. Geodetic evidence for rifting in Afar, 2. Vertical
286 displacements, Earth Planet. Sci. Lett., 48(2), 363–370.
287 Tesfaye, S., Harding, D. J., & Kusky, T. M. 2003. Early continental breakup boundary and migration
288 of the Afar triple junction, Ethiopia. Geological Society of America Bulletin, 115(9), 1053–
289 1067. https://doi.org/10.1130/B25149.1
290 Thielicke, W., & Stamhuis, E. J. 2014. PIVlab—Towards user-friendly, affordable and accurate
291 digital particle image velocimetry in MATLAB. Journal of Open Research Software, 2, e30.
292 https://doi.org/10.5334/jors.bl
293 Varet, J. 2018. Geology of Afar (East Africa) (p. 336). Springer. https://doi.org/10.1007/978-3-319-
294 60865-5
295 Wolfenden, E., Ebinger, C., Yirgu, G., Deino, A., & Ayalew, D. 2004. Evolution of the northern Main
296 Ethiopian Rift: Birth of a triple junction. Earth and Planetary Science Letters, 224(1–2), 213–
297 228. https://doi.org/10.1016/j.epsl.2004.04.022
298 Wright, T. J., Sigmundsson, F., Pagli, C., Belachew, M., Hamling, I. J., Brandsdóttir, B., ... & Calais,
299 E. 2012. Geophysical constraints on the dynamics of spreading centres from rifting episodes
300 on land. Nature Geoscience, 5(4), 242-250. https://doi.org/10.1038/ngeo1428
301 Wright, T., Ebinger, C., Biggs, J., Ayele, A., Yirgu, G., Keir, D., Stork, A. 2006. Magma-maintained
302 rift segmentation at continental rupture in the 2005 Afar dyking episode. Nature 442, 291–
303 294. https://doi.org/10.1038/nature04978

Zwaan, F., Chenin, P., Erratt, D., Manatschal, G., & Schreurs, G. 2021. Complex rift patterns, a result of interacting crustal and mantle weaknesses, or multiphase rifting? Insights from analog models. Solid Earth, 12(7), 1473-1495. https://doi.org/10.5194/se-12-1473-2021

FIGURE CAPTIONS

Figure 1. Tectonic setting of the Afar depression (modified from Keir et al., 2013, after Manighetti et al., 2001). A) Simplified fault pattern and main volcanic centers. Inset in the top right shows a sketch of the East African Rift and its plate tectonic setting. KR: Kenya Rift; MER: Main Ethiopian Rift; TC: Tanzanian Craton; TD: Turkana Depression; WB: Western Branch. Bottom right inset shows the plate tectonic setting of the Afar depression. Af: African plate; Ar: Arabian plate; GoA: Gulf of Aden; So: Somalian plate; TJ: Triple Junction; IM: Immino Graben. B) Detail of the T-shaped fault interaction in central Afar. C) Rose diagram (10° bin) of fault segments. Considered structures are those included in the dashed rectangle in A.

Figure 2. Final results of the best fit analog model (model A-OR-6 modified from Maestrelli et al., 2022; see supplementary Fig. S2 for details). A) Fault pattern superimposed on the topography (DEM) of the model surface at the end of deformation. The model is rotated 32° clockwise to be directly comparable to Afar. B) Close up of the triple junction area showing the typical T-shaped fault interactions. C) Rose diagram of fault distribution in B calculated as in Fig. 1C.

Figure 3. Evolution of T-shaped fault interaction at the model triple junction (area covers the inset in Fig. 2). White bars indicate the displacement on the faults, calculated as in Philippon et al. (2015). Vectors in the box show the total extension between the three plates. White arrow shows northern plate movement during 1st deformation stage. Dashed gray lines mark plate boundaries position.

Figure 4. Model to nature comparison of deformation kinematics. A) Comparison between velocity vectors in the model (black arrows) and GNSS data in Afar (yellow arrows denote the measured data; grey arrows show motion data interpolated from measured ones on a 5x5 km grid). Velocity vectors (black arrows) in the models are obtained from PIV analysis (see supplementary Fig. S4), following the methods described in Maestrelli et al., (2021a,b). GNSS vectors and model velocity vectors were calculated considering, respectively, a fixed Africa plate and a fixed SW model plate. B) Comparison between T-axes from earthquakes in Afar (red lines; derived from gCMT catalogue, Ekström et al., 2012) and T-axes from the model calculated as in Philippon et al. (2015). The dashed box encloses T-axes resulting from earthquakes related to the Dabbahu dike sequence. C) Scheme showing the correspondence between scaled analog model boundaries and nature. MP1, MP2 and MP3: moving plates, cf. Fig. S2.

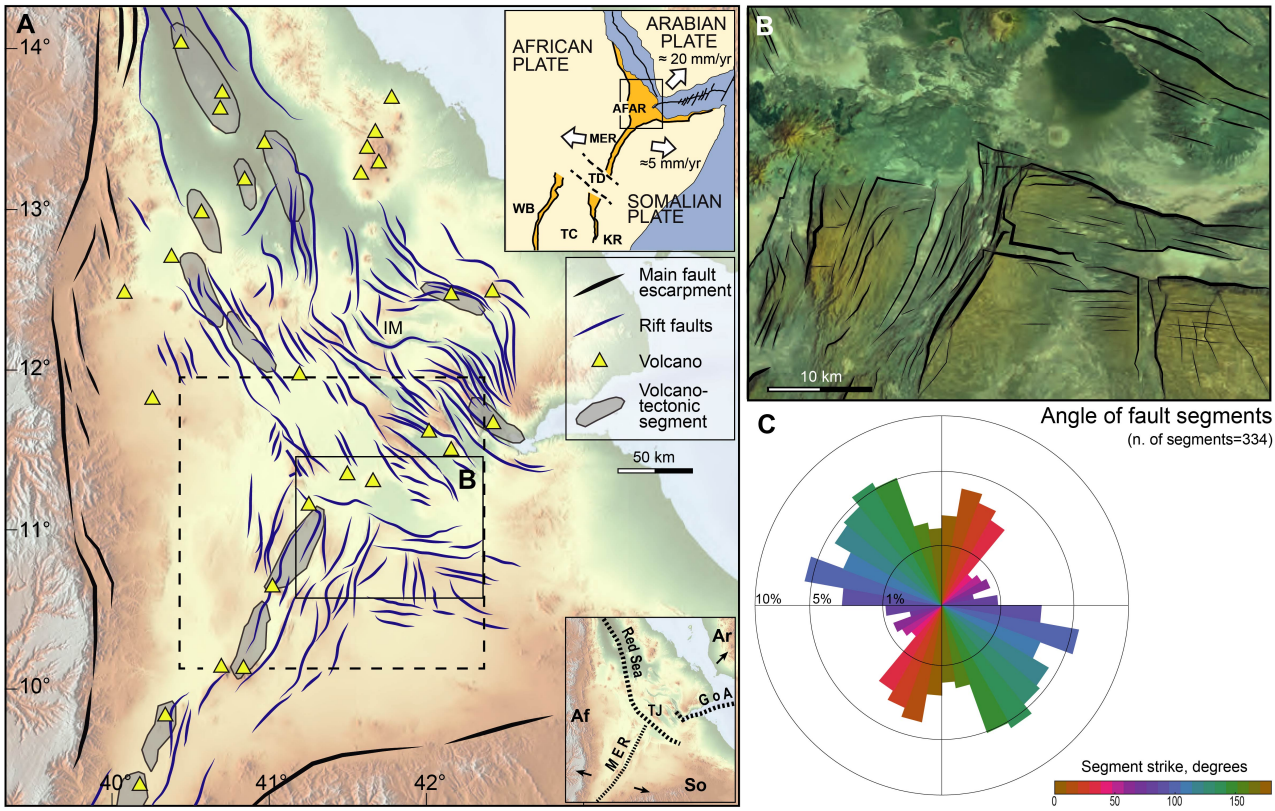

371

372 **Figure 1.**

373

374

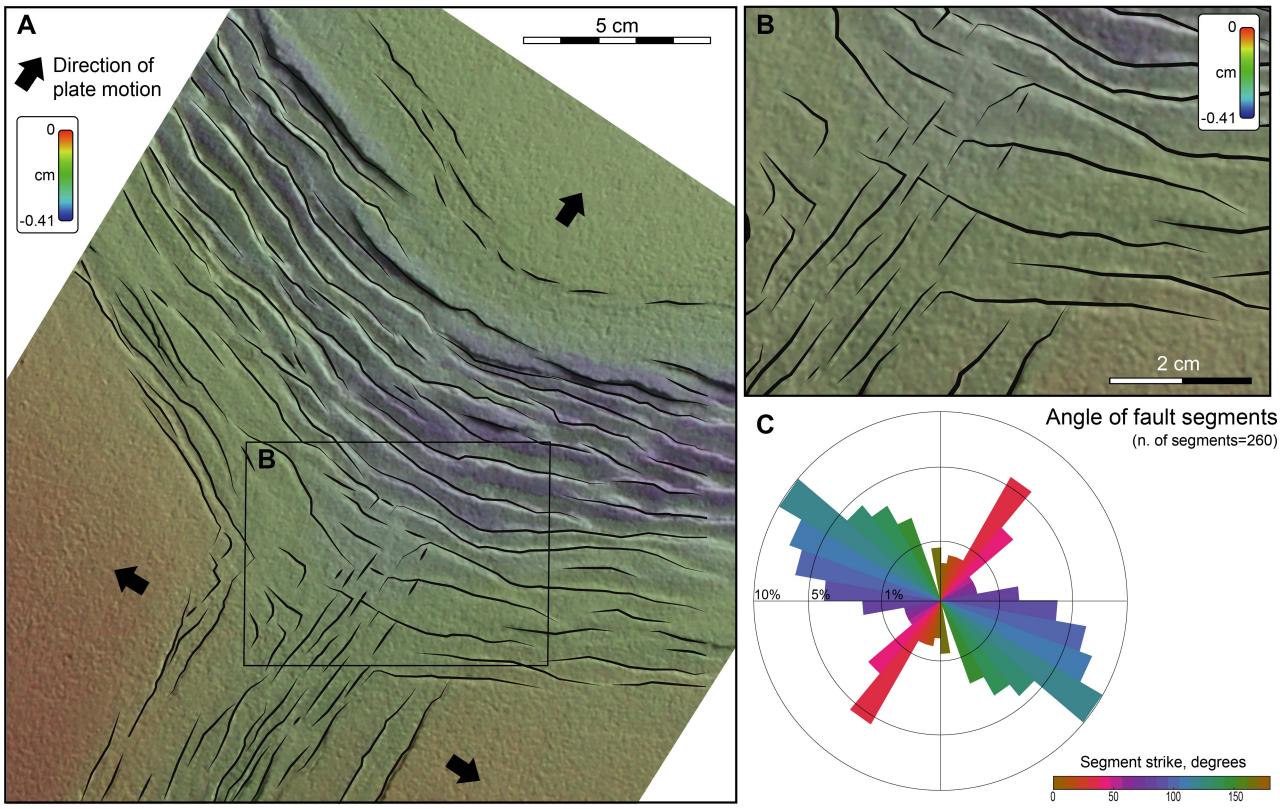

375

376 **Figure 2.**

377

378

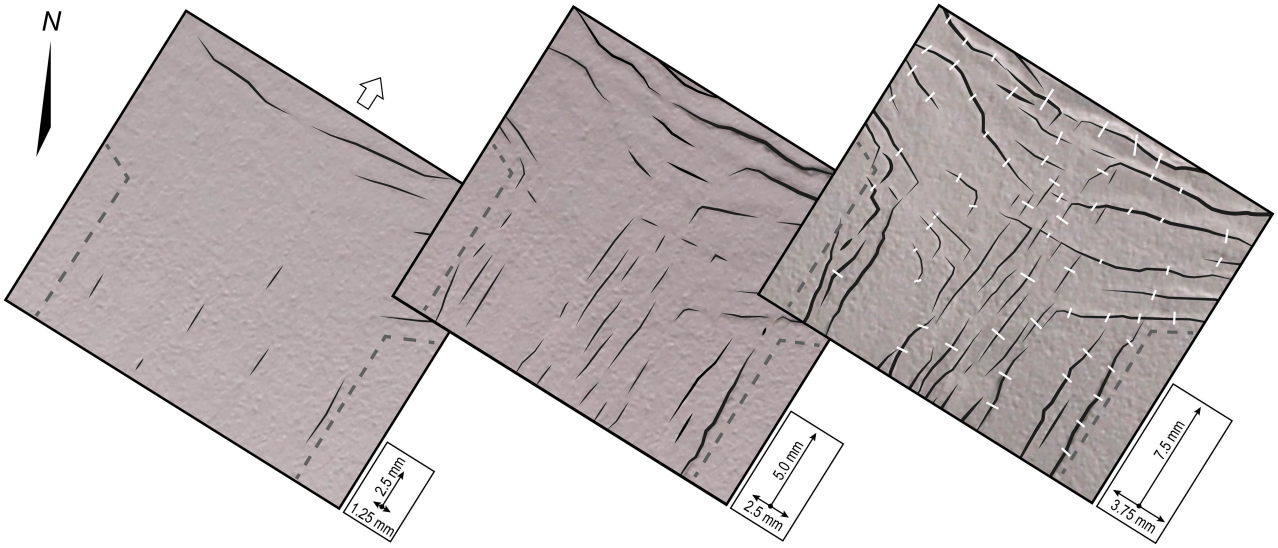

379

380 **Figure 3.**

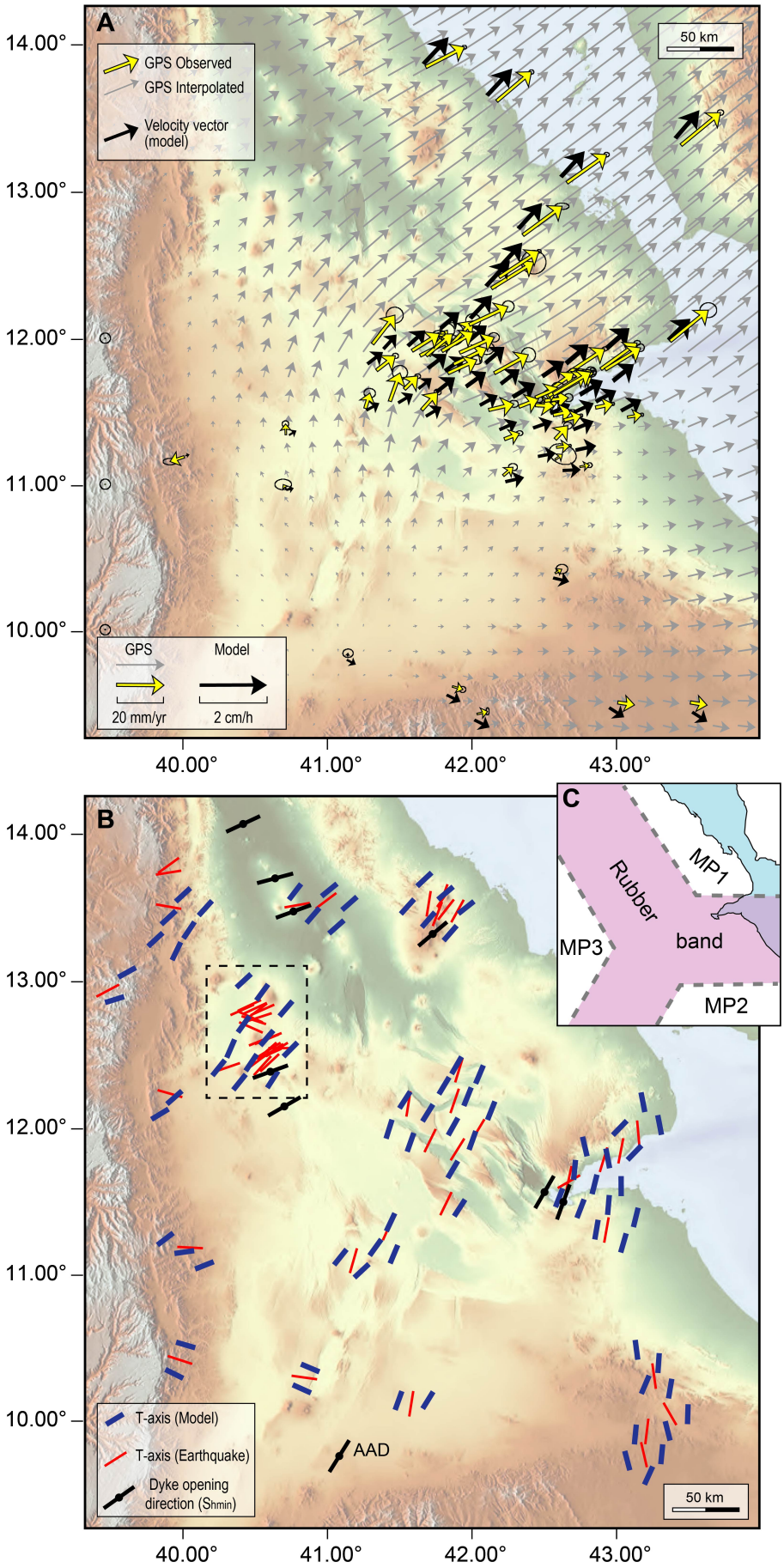
A
GPS Observed
GPS Interpolated
Velocity vector (model)
50 km
GPS
Model
20 mm/yr
2 cm/h
B
T-axis (Model)
T-axis (Earthquake)
Dyke opening direction (Shmin)
AAD
50 km
C
Rubber
band
MP1
MP2
MP3
14.00°
13.00°
12.00°
11.00°
10.00°
40.00°
41.00°
42.00°
43.00°

Figure 4.